28
3-4-81
Sent to NTIS

(2)
R2404

ornl

MASTER

ORNL/TM-7602

OAK RIDGE NATIONAL LABORATORY

UNION CARBIDE

Supplementary Neutron Flux Calculations for the ORNL Pool Critical Assembly Pressure Vessel Facility

R. E. Maerker
P. J. Maudlin

OPERATED BY
UNION CARBIDE CORPORATION
FOR THE UNITED STATES
DEPARTMENT OF ENERGY

DISTRIBUTION OF THIS DOCUMENT IS UNLIMITED

ORNL/TM-7602

DISCLAIMER

This report was prepared as an account of work sponsored by an agency of the United States Government. Neither the United States Government nor any agency thereof, nor any of their employees, makes any warranty, express or implied, or assumes any legal liability or responsibility for the accuracy, completeness, or usefulness of any information, apparatus, product, or process disclosed, or represents that its use would not infringe privately owned rights. Reference herein to any specific commercial product, process, or service by trade name, trademark, manufacturer, or otherwise, does not necessarily constitute or imply its endorsement, recommendation, or favoring by the United States Government or any agency thereof. The views and opinions of authors expressed herein do not necessarily state or reflect those of the United States Government or any agency thereof.

Contract No. W-7405-eng-26

Engineering Physics Division

SUPPLEMENTARY NEUTRON FLUX CALCULATIONS FOR THE ORNL POOL CRITICAL ASSEMBLY PRESSURE VESSEL FACILITY

R. E. Maerker

P. J. Maudlin*

Date Published - February 1981

*Present address: Los Alamos Scientific Laboratory

Prepared by the
OAK RIDGE NATIONAL LABORATORY
Oak Ridge, Tennessee 37830
operated by
UNION CARBIDE CORPORATION
for the
DEPARTMENT OF ENERGY

DISTRIBUTION OF THIS DOCUMENT IS UNLIMITED

CONTENTS

LIST OF TABLES

LIST OF FIGURES

ABSTRACT

A three-dimensional Monte Carlo calculation was performed to estimate the neutron flux in the 8/7 configuration of the ORNL Pool Critical Assembly Pressure Vessel Facility. The calculational tool was the multigroup transport code MORSE operated in the adjoint mode. The MORSE flux results compared well with those using a previously adopted procedure for constructing a three-dimensional flux from one- and two-dimensional discrete ordinates calculations using the DOT-IV code. This study concluded that use of these discrete ordinates constructions in previous calculations is sufficiently accurate and does not account for the existing discrepancies between calculation and experiment.

I. INTRODUCTION

The Pool Critical Assembly Pressure Vessel Facility (PCA-PVF or more simply PCA) was instituted to serve as a benchmark for validating calculational procedures in predicting neutron fluences in reactor pressure vessels for estimation of damage.[1] A description of the various calculations carried out for the PCA by an international group of analysts is presented in Ref. 2. Included in this reference is a comparison of the calculational results with radiometric and neutron spectroscopy measurements in the PCA, comparing neutron spectra and various saturated reaction rates. Unfortunately, a sizable underprediction (~20%) seems to persist throughout a majority of the calculation-versus-experimental comparisons that is larger than the combination of all the perceived uncertainties. The source of this discrepancy is presently a point of speculation and controversy.

A possible source of this discrepancy is the treatment of the three-dimensional PCA geometry by two-dimensional calculational methods adjusted in some manner for the third dimension. With one exception, all the analysts use one- and two-dimensional discrete ordinates transport methods and incorporate adjustments. The one exception uses a continuous energy Monte Carlo code to perform the true three-dimensional calculation, but unfortunately reports results with fairly large statistical uncertainties (comp. Ref. 2).

A tenable approach first proposed by Combustion Engineering[2] and adopted by Oak Ridge[3] for scaling the two-dimensional calculations is indicated by the following space, energy and angular dependent flux relationship:

$$\phi(x,y,z,E,\vec{\Omega}) \cong \phi(x,y,E,\vec{\Omega}) \left[\frac{\phi(y,z,E,\vec{\Omega})}{\phi(y,E,\vec{\Omega})}\right], \tag{1a}$$

or more conveniently

$$\phi_{XYZ} \cong \phi_{XY} \left|\phi_{YZ}/\phi_{Y}\right|, \tag{1b}$$

where in the present application this approximation is limited to y centerline values (i.e., for x = z = 0 see Fig. 1). Equation (1) states that a three-dimensional flux, ϕ_{XYZ}, can be constructed from information obtained from two two-dimensional calculations, ϕ_{XY} and ϕ_{YZ}, and a one-dimensional calculation, ϕ_Y, by simply scaling the ϕ_{XY} calculation by the properly normalized z-correction term given in the brackets. The ϕ_{XY}, ϕ_{YZ}, and ϕ_Y calculations have geometry of infinite extent in the z-direction, x-direction, and xz-plane, respectively.

In the PCA calculations, the source per unit height for the midplane XY calculation is normalized in such a way that when intergrated over x, y, and z yields a value of unity (i.e., there is one fission neutron in the core). The effects of finite z and the source distribution in z appear as the correction term ϕ_{YZ}/ϕ_Y. This ratio can be calculated using much simpler YZ and Y geometries than used to calculate ϕ_{XY}, but the y dimensions and source distribution in y must be the same for both the YZ and Y geometries. The normalization of the source distribution in z for the ϕ_{YZ} calculation relative to the source per unit height for the ϕ_Y calculation must also be set equal to the ratio of the integrals over the two z-distributions after their maxima have been adjusted to agree (see Section II). Of course, the approximation of Eq. (1) disregards possible three-dimensional coupling effects, such as the impact of finite x-dimension effects on the z-correction term. Note that in Ref. 2 other approaches for adjusting two-dimensional calculations to approximate ϕ_{XYZ} have also been used, e.g., space-energy dependent bucklings.

The object of this work is to evaluate approximation (1) by calculating directly the true flux ϕ_{XYZ} via a Monte Carlo transport code, and to compare these results with the constructed flux represented by the RHS of Eq. (1). For this purpose, the multigroup Monte Carlo code MORSE[4] is used to estimate ϕ_{XYZ}, and the DOT-IV[5] discrete ordinates code is used to determine ϕ_{XY}, ϕ_{YZ}, and ϕ_Y.

First, a physical description of the PCA-PVF in terms of geometry and materials is provided in Sect. II, with a more detailed description of the calculational methods in Sect. III. Section IV presents results

from the investigations of the validity of approximation (1). These feature three-dimensional Monte Carlo calculations of the neutron flux as a function of space and energy. Section V summarizes the conclusions that may be drawn from these investigations.

II. PHYSICAL DESCRIPTION OF THE PCA

The PCA was designed to simulate within intensity constraints the geometry and materials that exist in a commercial light water reactor pressure vessel. The geometry is illustrated in Fig. 1 showing an arrangement of slabs which represent the reactor core, appropriate water gaps, a thermal shield, and the pressure vessel wall. This geometry is a slight simplification of the actual configuration described in Ref. 1, but does not compromise the analysis of Sect. IV. The dimensions of the slabs and water gaps given in Fig. 1 are in units of centimeters. Note that this particular arrangement of the PCA is referred to in Refs. 1 and 2 as the "8/7 configuration," since the two major water gaps are roughly 8 cm and 7 cm wide. This configuration was chosen over the "12/13 configuration," which was more extensively measured,[2] to reduce the computational cost.

A reflective boundary condition exists on the left face of the core zone (i.e., the xz plane at y = 0), and a vacuum boundary condition exists on the right face of the pressure vessel (i.e., the xz plane at y = 66.7 cm). All remaining slab faces are reflected with water.

Seven neutron flux detectors are designated in Fig. 1 as "D1" through "D7," with their coordinates given in the detector location table in the lower right corner. These detectors represent spatial locations where the neutron flux is calculated. Note that they all lie on the y axis.

A material description of the PCA is presented in Table 1, giving the material name, media number(s), composition of the material, and associated number densities in columns one through four, respectively. These material compositions are slightly different from the actual compositions described in Ref. 1; for example, the core composition should contain some ^{235}U. However, these simplications represent modeling convenience and take advantage of prior cross section preparation that again do not compromise the analysis of Sect. IV.

The spatial zones in Fig. 1 where the materials of Table 1 homogeneously exist are identified by the cross-section media numbers "M1" through "M8." For example, the core zone in Fig. 1, which is composed

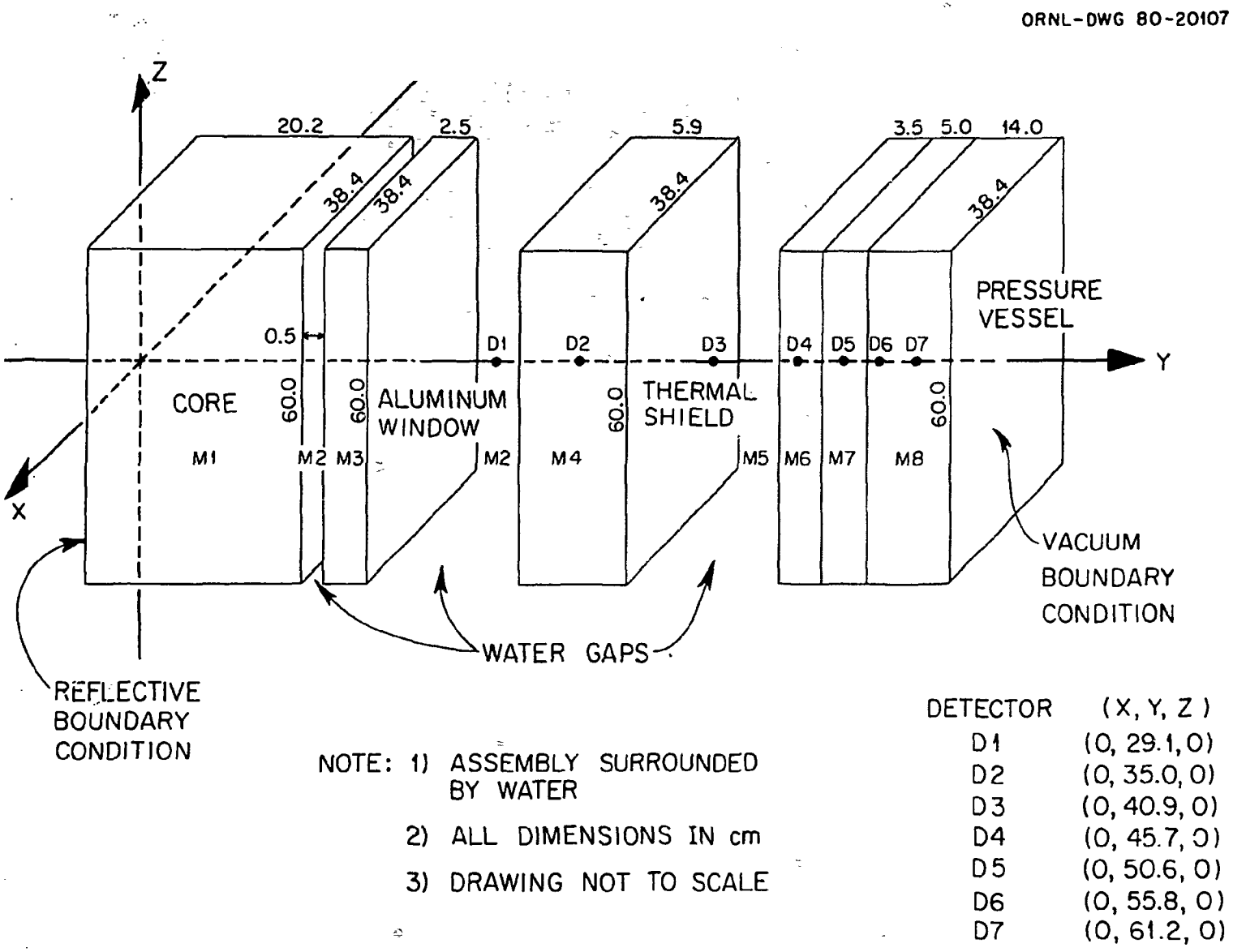

Fig. 1. Modeling geometry for the pool critical assembly.
In the 8/7 configuration, the two large water gaps were 8.4- and 6.7-cm wide respectively.

Table 1. Material description of the pool critical assembly

Material	Media number	Composition by volume	Number density (atoms/b-cm)
Core material	M1	H (45%)	0.0361
		O (23%)	0.0180
		Al (32%)	0.0255
Water	M2, M5	H (67%)	0.0670
		O (33%)	0.0335
Aluminum	M3	Al (100%)	0.0602
Stainless steel	M4	Fe (70%)	0.0594
		Cr (20%)	0.0169
		Ni (9%)	0.0079
		Mn (1%)	0.0012
Carbon steel	M6, M7, M8	Fe (98%)	0.0837
		Mn (1%)	0.0005
		C (1%)	0.0010

of H_2O and Al as indicated in Table 1, is designated as medium M1, and hence is described by a single set of neutron cross-sections. The pressure vessel, which is composed of carbon steel, is represented by three different media (i.e., M6, M7, and M8), and hence is described by three different sets of zone-flux weighted neutron cross-sections. Further discussion of these cross-section media is given in the next section.

The three-dimensional neutron source distribution for the core zone has the following form:

$$S(x,y,z,E,\vec{\Omega}) = S_{XYZ}(x,y,z)S_E(E)S_\Omega(\vec{\Omega}) \ , \tag{2}$$

where each of the density functions on the RHS of Eq. (2) are normalized to unity, and where

$$S_{XYZ}(x,y,z) = s_{XY}(x,y)s_Z(z) \ . \tag{3}$$

The source distribution in the z direction has a cosine form:

$$s_Z(z) = \cos(B_Z z) \ , \quad -L_Z/2 \leq z \leq L_Z/2 \ . \tag{4}$$

The buckling B_Z has been measured for the PCA and has the value[1] 0.0442 cm^{-1} ± 2.8%. The core height L_Z is seen from Fig. 1 to be 60 cm.

The source distribution over the xy plane at z = 0, $s_{XY}(x,y)$, has also been measured[1] and is given in Fig. 2 in a discrete form, where the values are such that S_{XYZ} integrates to unity. Quarter core symmetry is assumed in Fig. 2, where the xy origin coincides with the xyz origin of Fig. 1.

In order to match the maxima of the two distributions at z = 0, the ratio of the source normalizations for the ϕ_{YZ} and ϕ_Y calculations must be

ORNL - DWG 80 20108

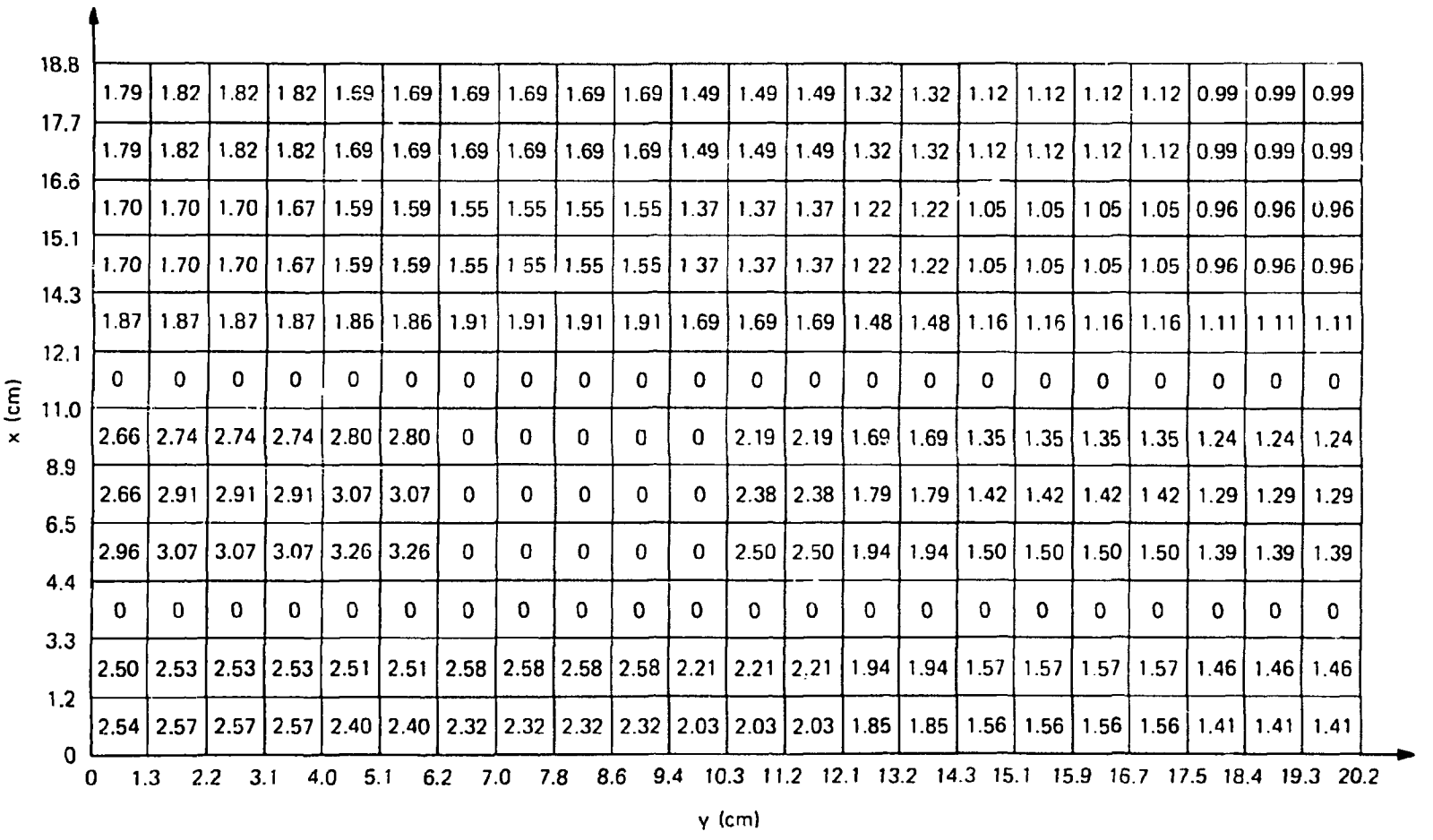

Fig. 2. Quarter core midplane neutron source distribution in units of 10^{-5} neutrons/s-cm^3.

$$\frac{\sin(B_Z L_Z/2)}{B_Z L_Z/2} = 0.7317 \ .$$

The source energy distribution, S_E, derived from ENDF/B-V Watt fission spectrum parameters for ^{235}U, is given in the 24 group representation used in this analysis in Table 2.

The source angular distribution, S_Ω, is assumed isotropic (i.e., $S_\Omega = 1/4\pi$).

Table 2. Neutron group structure and source energy distribution

Group	Upper energy (eV)	Source fraction
1	1.9640E 07	5.5841E-04
2	1.1052E 07	4.7115E-03
3	8.1873E 06	2.0686E-02
4	6.0653E 06	8.1625E-02
5	4.0657E 06	1.0943E-01
6	3.0119E 06	6.6245E-02
7	2.5924E 06	9.4196E-02
8	2.1225E 06	7.1393E-02
9	1.8268E 06	9.1620E-02
10	1.4957E 06	8.3815E-02
11	1.2246E 06	1.0632E-01
12	9.0718E 05	1.0401E-01
13	6.0810E 05	7.9861E-02
14	3.6883E 05	4.5758E-02
15	2.1280E 05	2.4181E-02
16	1.1109E 05	4.7754E-03
17	8.6517E 04	3.3285E-03
18	6.7379E 04	4.7356E-03
19	3.4307E 04	9.2599E-04
20	2.6058E 04	1.2761E-03
21	1.1709E 04	3.7397E-04
22	5.5308E 03	1.2177E-04
23	2.6126E 03	5.6560E-05
24	4.1399E-01	0.0
Total		1.000E-00

III. CALCULATIONAL METHODS

As mentioned in Sect. I, the MORSE[4] code was selected to estimate ϕ_{XYZ} for the PCA. This code is a multipurpose neutron and gamma-ray transport Monte Carlo code that has time dependence and three-dimensional geometry capability. Standard multigroup cross sections such as those used in discrete ordinates codes can be used as input. Also a calculation can be performed in either the forward or adjoint mode.

As was also mentioned in Sect. I, the DOT-IV[5] code is used to determine ϕ_{XY}, ϕ_{YZ} and ϕ_{Y} for the PCA. This code is a two-dimensional discrete ordinates transport code that has the flexibility to address many deep penetration shielding problems. The use of this code to calculate ϕ_{Y} by inserting appropriate reflecting surfaces is preferable to the use of ANISN for this purpose, since consistent angular quadratures can be employed.

A 24-group cross section library was generated for the PCA using the AMPX-II[6] code system. Starting with a 174-group AMPX master library obtained from ENDF/B-V, Bondarenko self-shielding factors derived from $(1/\Sigma_T)$ weighting for each of the two steels (i.e., stainless steel for the thermal shield and carbon steel for the pressure vessel) were applied prior to a one-dimensional discrete ordinates calculation of the neutron flux. This flux was then used in a subsequent cross section collapsing process which yielded a P3, 24-group, spatially dependent library having the group structure given in Table 2. The spatial dependence of the cross sections is indicated by the different media numbers in Fig. 1 and Table 1. Both the MORSE and DOT-IV calculations use the same 24-group cross section library and neutron source energy distribution given in Table 2. Note that these 24-group DOT calculations are not the 51-group DOT calculations used in the PCA analysis by ORNL.[2]

The PCA problem features a large neutron source volume emitting neutrons which impinge upon point detectors at locations D1 through D7 in Fig. 1. The penetration distance from the core to detector D7 is roughly 10 mean-free-paths. Running MORSE in the forward mode with point detector estimators is prohibitively expensive. The use of boundary crossing or finite detector volume estimators reduces the

expense substantially, but yields troublesome averaged fluxes rather than point fluxes. Conversely, running MORSE in the adjoint mode not only permits the use of a track length estimator in the entire core volume, but also avoids the singularity and associated poor statistics of a point detector estimator. Of course the disadvantage of the adjoint mode is that a separate calculation is needed for each detector location, and also for each energy group for reliable statistics. However, for the PCA problem the advantages of operating in the adjoint mode were found to far outweigh this disadvantage. Hence, the adjoint mode with only standard biasing techniques (i.e., Russian roulette, splitting, and pathlength stretching) was selected for the ϕ_{XYZ} calculations presented in Sect. IV.

IV. INVESTIGATIONS

The investigations presented in this section are restricted to an analysis of only the first twelve groups of Table 2, i.e., only neutrons above 0.6 MeV. This range of energies is sufficient, however, to calculate all the threshold activation rates measured in the PCA. Therefore, unless otherwise specified, the fluxes given in the tables and figures below are "total" fluxes integrated over the top twelve groups.

The units chosen for the fluxes presented in this report (which are really fluences) are neutrons per square centimeter per source neutron emitted from a cubic centimeter of the core zone. This particular source normalization arises naturally from the Monte Carlo scoring procedure over the core volume as well as for treating the use of infinite dimensions in the DOT calculations. Multiplication of these results by the space-average neutron source density (in units of neutrons per second per cubic centimeter) would yield absolute fluxes.

Various one- and two-dimensional flux calculations [i.e., ϕ_{XY}, ϕ_{YZ} and ϕ_{Y} of Eq. (1)] are presented in Table 3 for all seven detectors. These fluxes are first calculated with DOT (columns two through four) and are then compared with MORSE results (columns five through seven). The uncertainties given with the MORSE results represent one standard deviation (σ), and are, of course, themselves estimates. The MORSE fluxes, when considered as a whole, compare well with the DOT fluxes: roughly 2/3 of the MORSE estimates fall within one σ of the DOT results. Hence, Table 3 serves to validate the equivalence of the two calculational tools (there is perhaps evidence of a small but unimportant bias) and provides confidence in the three-dimensional results presented next.

Table 4 compares a three-dimensional MORSE estimate of the total flux with the DOT construction given by Eq. (1) for each detector. The relative disagreement between the MORSE and DOT results (MORSE-DOT/DOT) is given in the last column. As indicated by this column, the disagreement between the fluxes is quite small — the largest difference being 5% for detector D6. Furthermore, these differences do not show any increasing or decreasing trend as a function of detector location. However, they do seem to be biased toward a positive value, i.e., the MORSE

Table 3. Neutron flux comparisons between DOT-IV and adjoint MORSE calculations for neutrons above 0.6 MeV

Detector	DOT-IV fluxes[a]			Adjoint MORSE fluxes[a]		
	ϕ_{XY}	ϕ_{YZ}	ϕ_{Y}	ϕ_{XY}	ϕ_{YZ}	ϕ_{Y}
D1	0.775	0.804	0.927	0.786 ± 0.6%[b]	0.815 ± 0.8%[b]	0.947 ± 1.7%[b]
D2	0.414	0.435	0.522			
D3	9.40×10^{-2}	9.96×10^{-2}	0.124		9.96×10^{-2} ± 1.9%	0.124 ± 5.8%
D4	5.96×10^{-2}	6.51×10^{-2}	8.55×10^{-2}			
D5	3.86×10^{-2}	4.51×10^{-2}	5.70×10^{-2}	3.96×10^{-2} ± 3.0%	4.35×10^{-2} ± 3.7%	6.54×10^{-2} ± 5.2%
D6	2.15×10^{-2}	2.36×10^{-2}	3.38×10^{-2}	2.27×10^{-2} ± 4.6%		
D7	1.12×10^{-2}	1.23×10^{-2}	1.82×10^{-2}	1.16×10^{-2} ± 5.6%	1.38×10^{-2} ± 7.4%	2.19×10^{-2} ± 8.3%

[a] Units: neutrons/cm^2/(source neutron/cm^3) for ϕ_{XY} and ϕ_{Y}, and neutrons/cm^2/(0.7317 source neutron/cm^3) for ϕ_{YZ}.

[b] Uncertainties are one σ.

Table 4. Three-dimensional flux comparisons for neutrons above 0.6 MeV

Detector	Adjoint MORSE[a] ϕ_{XYZ}	DOT-IV Construction[a] $\phi_{XY}(\phi_{YZ}/\phi_{Y})$	Relative error (%)
D1	0.682 ± 0.5%[b]	0.672	1.5 ± 0.5[b]
D2	0.346 ± 0.8%	0.345	0.3 ± 0.8
D3	7.77×10^{-2} ± 1.1%	7.55×10^{-2}	2.9 ± 1.1
D4	4.74×10^{-2} ± 1.3%	4.54×10^{-2}	4.4 ± 1.4
D5	2.85×10^{-2} ± 2.1%	2.81×10^{-2}	0.7 ± 2.1
D6	1.58×10^{-2} ± 3.4%	1.50×10^{-2}	5.3 ± 3.6
D7	7.53×10^{-3} ± 3.5%	7.57×10^{-3}	-0.5 ± 3.5

[a] Units: neutrons/cm^2/(source neutron/cm^3).

[b] Uncertainties are one σ.

fluxes are just slightly larger than the DOT construction, as was first observed in Table 3.

Figure 3 shows the total fluxes of Tables 3 and 4 plotted as a function of y. The units for ϕ_{YZ} as plotted are neutrons/cm^2/(0.7317 source neutron/cm^3), while those for the others are neutrons/cm^2/source neutron/cm^3. These fluxes are seen to attenuate more rapidly in the water gaps than in the thermal shield and pressure vessel. This is the expected behavior despite the fact that $\Sigma_t^{Fe} > \Sigma_t^{H_2O}$ since the energy loss per hydrogen scattering is very large. The differences between the relative magnitudes of these fluxes is due to the different leakage losses and source distributions. The ϕ_{XYZ} calculation contains three-dimensional leakage and thus has the smallest magnitude. On an equal source neutron density basis, $\phi_{YZ} > \phi_Y$ at the first five detectors because the central source region is more important than the wings in contributing to these fluxes. On the same basis, $\phi_{YZ} \approx 1.5\ \phi_{XY}$ because there is less leakage in the z-direction than in the x-direction. The DOT constructed flux is not shown in Fig. 3 since it is virtually identical to that shown for the MORSE calculation.

One- and two-dimensional group flux results using DOT are given in Table 5 for the first twelve groups at detector location D5, which corresponds to the "T/4" location. A summation over groups of these fluxes would yield the total flux values for detector D5 in Table 3. The DOT fluxes from Table 5 are then assembled to again construct the three-dimensional flux proposed by Eq. (1). Table 6 presents a comparison between this construction and the three-dimensional MORSE result, and gives the relative difference between the two. The MORSE estimates compare well with the DOT approximation for the first nine groups, but this agreement deteriorates somewhat for the last three. The lack of agreement here is more likely due to statistical fluctuation than to any real difference since the total fluxes from Table 4 are in agreement. Observe also that the MORSE group fluxes sum to a total flux of 2.69×10^{-2} which is below the Table 4 value 2.85×10^{-2}. With these considerations kept in mind then, Table 6 indicates good spectral agreement between MORSE and DOT as well.

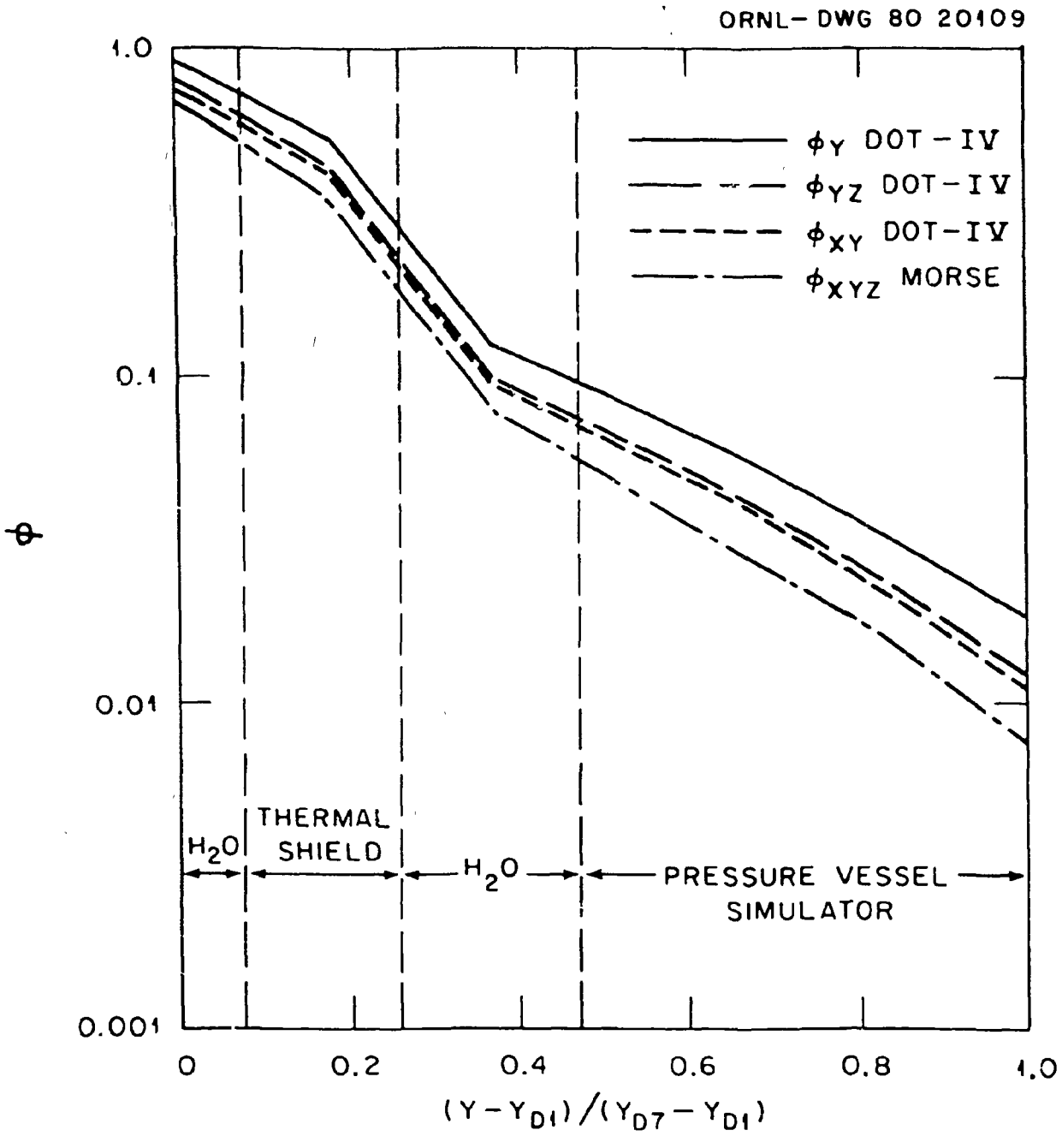

Fig. 3. Total neutron flux comparisons. (see text for flux units)

Table 5. DOT-IV neutron group fluxes at detector D5

Energy group	DOT-IV fluxes[a]		
	ϕ_{XY}	ϕ_{YZ}	ϕ_{Y}
1	2.17×10^{-5}	2.23×10^{-5}	3.15×10^{-5}
2	1.41×10^{-4}	1.45×10^{-4}	2.10×10^{-4}
3	4.77×10^{-4}	4.95×10^{-4}	6.72×10^{-4}
4	1.31×10^{-3}	1.38×10^{-3}	1.83×10^{-3}
5	1.42×10^{-3}	1.51×10^{-3}	1.98×10^{-3}
6	1.37×10^{-3}	1.46×10^{-3}	1.93×10^{-3}
7	2.69×10^{-3}	2.87×10^{-3}	3.79×10^{-3}
8	1.99×10^{-3}	2.13×10^{-3}	2.82×10^{-3}
9	3.55×10^{-3}	3.81×10^{-3}	5.08×10^{-3}
10	3.82×10^{-3}	4.10×10^{-3}	5.47×10^{-3}
11	7.38×10^{-3}	7.98×10^{-3}	1.09×10^{-3}
12	1.44×10^{-2}	1.56×10^{-2}	2.21×10^{-2}

[a] Units: neutrons/cm^2/(source neutron/cm^3) for ϕ_{XY} and ϕ_{Y}, and neutrons/cm^2/(0.7317 source neutron/cm^3) for ϕ_{YZ}.

Table 6. Three-dimensional group flux comparisons at detector D5

Energy group	Adjoint MORSE[a] ϕ_{XYZ}	DOT-IV Construction[a] $\phi_{XY}(\phi_{YZ}/\phi_{Y})$	Relative error (%)
1	$1.56 \times 10^{-5} \pm 3.0\%$[b]	1.54×10^{-5}	1.3 ± 3.0[b]
2	$1.04 \times 10^{-4} \pm 1.9\%$	1.02×10^{-4}	2.0 ± 1.9
3	$3.62 \times 10^{-4} \pm 3.5\%$	3.51×10^{-4}	3.1 ± 3.6
4	$9.97 \times 10^{-4} \pm 2.9\%$	9.88×10^{-4}	0.9 ± 2.9
5	$1.07 \times 10^{-3} \pm 3.7\%$	1.08×10^{-3}	-0.9 ± 3.7
6	$9.83 \times 10^{-4} \pm 3.6\%$	1.04×10^{-3}	-5.5 ± 3.4
7	$1.99 \times 10^{-3} \pm 2.4\%$	2.04×10^{-3}	-2.4 ± 2.3
8	$1.44 \times 10^{-3} \pm 2.3\%$	1.50×10^{-3}	-4.0 ± 2.2
9	$2.79 \times 10^{-3} \pm 2.5\%$	2.66×10^{-3}	4.9 ± 2.6
10	$2.69 \times 10^{-3} \pm 2.3\%$	2.86×10^{-3}	-5.9 ± 2.2
11	$4.88 \times 10^{-3} \pm 2.4\%$	5.40×10^{-3}	-9.6 ± 2.2
12	$9.60 \times 10^{-3} \pm 2.2\%$	1.02×10^{-2}	-5.9 ± 2.1

[a] Units: neutrons/cm^2/(source neutron/cm^3).

[b] Uncertainties are one σ.

The energy dependent information of Tables 5 and 6 is next converted into the neutron energy spectra presented in Fig. 4. This spectral display of the various DOT and MORSE group fluxes (i.e., ϕ_Y, ϕ_{XY}, ϕ_{YZ}, and ϕ_{XYZ}) is plotted over the first twelve groups. The area under each of these curves integrates to unity. The mean fission neutron energy of 2 MeV is also indicated in the figure. The various spectra behave in the classical fashion below the fission source (i.e., in groups 10, 11, and 12): the smaller the leakage loss the softer the spectrum. Hence, ϕ_Y which has the least leakage is the softest, whereas ϕ_{XYZ} which has the most leakage is the hardest. The other two spectra fall somewhere in between. The high value for ϕ_{XYZ} in group 9 is the result of the statistical fluctuations in groups 9 through 12 observed in Table 6 and discussed above. Note that, since the leakage losses in the XY and YZ geometries are relatively close in value, the corresponding spectra are very similar.

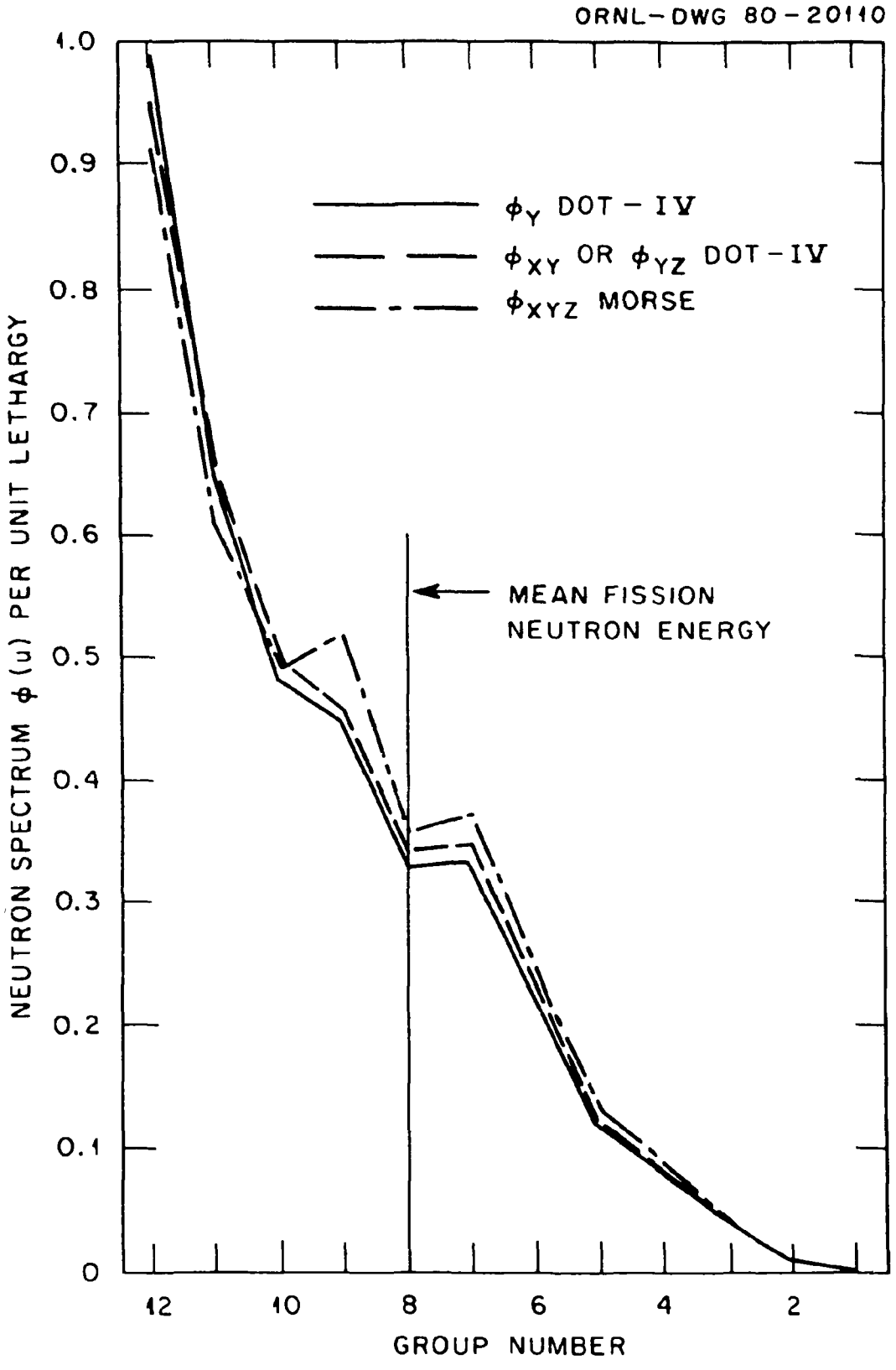

Fig. 4. Neutron energy spectrum comparisons

V. CONCLUSIONS

Recalling that the object of this work was to evaluate the DOT approximation represented by Eq. (1), the investigations of Sect. IV clearly validate the use of this approximation over the PCA space and energy domain studied (i.e., over all y in the 8/7 configuration for $x = z = 0$ and $E > 0.6$ MeV). Based on this conclusion, use of approximation (1) for somewhat less restrictive domains of x, y and z and $E < 0.6$ MeV is most likely justified. In particular, it should apply to the centerline detectors in the 12/13 configuration.

Let us further note that the combined three-dimensional aspects of the PCA geometry and source distribution apparently are separable and cancel out in the DOT construction of Eq. (1). Hence, the proposal in Sect. I that the discrepancy between PCA-PVF measurements and calculations is most likely due to the neglect of three-dimensional coupling effects, implied by the use of Eq. (1), is shown unfounded by this work. Apparently, the source of this discrepancy lies elsewhere.

ACKNOWLEDGMENTS

The authors acknowledge with gratitude the suggestions and advice of J. S. Tang and M. B. Emmett during the course of this work. This research was mutually funded by the Nuclear Regulatory Commission and the Electric Power Research Institute under ongoing analytical programs with the Oak Ridge National Laboratory.

REFERENCES

1. Technical Letter for the PCA "Blind Test," L. Miller, F. B. K. Kam, and A. Fabry, Oak Ridge National Laboratory, May 1979.
2. F. W. Stallmann, F. B. K. Kam, J. F. Eastham, and C. A. Baldwin, "Reactor Calculation 'Benchmark' PCA Blind Test Results," ORNL/NUREG/TM-428, Oak Ridge National Laboratory (1981).
3. J. J. Wagschal, R. E. Maerker, and B. L. Broadhead, "LWR-PV Damage Estimate Methodology," presented at the 1980 Advances in Reactor Physics and Shielding Conference, Sun Valley, Idaho (1980).
4. M. B. Emmett, "The MORSE Monte Carlo Radiation Transport Code System," ORNL-4972, Oak Ridge National Laboratory (1975).
5. W. A. Rhoades, D. B. Simpson, R. L. Childs, and W. W. Engle, "The DOT-IV Two Dimensional Discrete Ordinates Transport Code with Space-Dependent Mesh and Quadrature," ORNL/TM-6529, Oak Ridge National Laboratory (1979).
6. N. M. Greene, W. E. Ford, III, et al., "AMPX: A Modular Code System for Generating Coupled Multigroup Neutron-Gamma Libraries from ENDF/B," ORNL/TM-3706, Oak Ridge National Laboratory (1976).